Science of the Total Environment 912 (2024) 169143

Contents lists available at ScienceDirect

Science of the Total Environment

journal homepage: www.elsevier.com/locate/scitotenv

Sequential use of a continuous-flow electrocoagulation reactor and a (photo)electro-Fenton recirculation system for the treatment of Acid Brown 14 diazo dye

Ömür Gökkuş [a], Enric Brillas [b], Ignasi Sirés [b,*]

[a] Department of Environmental Engineering, Erciyes University, 38039 Kayseri, Türkiye
[b] Laboratori d'Electroquímica dels Materials i del Medi Ambient, Departament de Ciència de Materials i Química Física, Secció de Química Física, Facultat de Química, Universitat de Barcelona, Martí i Franquès 1-11, 08028 Barcelona, Spain

HIGHLIGHTS

- Total color decay of Acid Brown 14 solutions in continuous-flow electrocoagulation (EC) with Fe
- Poor mineralization by EC process, although greater in chloride medium
- Best EC conditions: 5A + 4C, pH = 4.0–10.0, I = 13.70 A, liquid flow rate 10 L h^{-1} and aeration
- Similar TOC decay by coupling EC to electro-Fenton (EF) at pH 3.0 and 50 mA cm^{-2} in all media
- Best mineralization in EC-photoelectro-Fenton (PEF) with UVA light, superior in sulfate medium

GRAPHICAL ABSTRACT

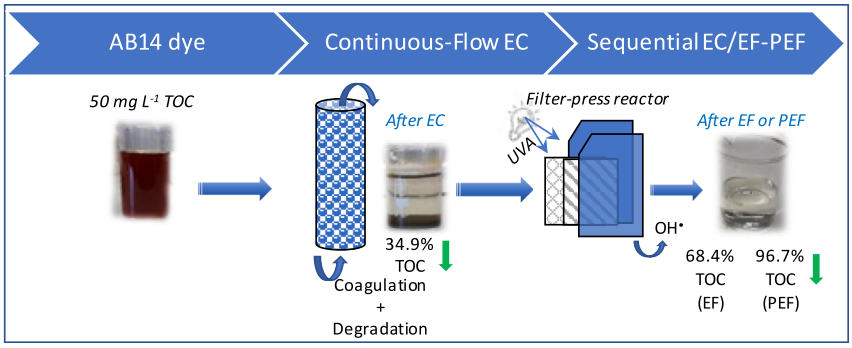

ARTICLE INFO

Editor: Qilin Wang

Keywords:
Acid Brown 14 diazo dye
Electrocoagulation
Electro-Fenton
Photoelectro-Fenton
Sequential process
Water treatment

ABSTRACT

The decolorization and TOC removal of solutions of Acid Brown 14 (AB14) diazo dye containing 50 mg L^{-1} of total organic carbon (TOC) have been first studied in a continuous-flow electrocoagulation (EC) reactor of 3 L capacity with Fe electrodes of ~110 cm^2 area each. Total loss of color with poor TOC removal was found in chloride, sulfate, and/or hydrogen carbonate matrices after 18 min of this treatment. The best performance was found using 5 anodes and 4 cathodes of Fe at 13.70 A and low liquid flow rate of 10 L h^{-1}, in aerated 39.6 mM NaCl medium within a pH range of 4.0–10.0. The effluent obtained from EC was further treated by electro-Fenton (EF) using a 2.5 L pre-pilot flow plant, which was equipped with a filter-press cell comprising a Pt anode and an air-diffusion cathode for H_2O_2 electrogeneration. Operating with 0.10–1.0 mM Fe^{2+} as catalyst at pH 3.0 and 50 mA cm^{-2}, a similar TOC removal of 68 % was found as maximal in chloride and sulfate media using the sequential EC-EF process. The EC-treated solutions were also treated by photoelectro-Fenton (PEF) employing a photoreactor with a 125 W UVA lamp. The sequential EC-PEF process yielded a much higher TOC reduction, close to 90 % and 97 % in chloride and sulfate media, respectively, due to the rapid photolysis of the final Fe(III)-carboxylate complexes. The formation of recalcitrant chloroderivatives from generated active chlorine limited

* Corresponding author.
E-mail address: i.sires@ub.edu (I. Sirés).

https://doi.org/10.1016/j.scitotenv.2023.169143
Received 1 October 2023; Received in revised form 3 December 2023; Accepted 4 December 2023
Available online 7 December 2023

the mineralization in the chloride matrix. For practical applications of this two-step technology, the high energy consumption of the UVA lamp in PEF could be reduced by using free sunlight.

1. Introduction

Water pollution is a global problem closely linked to the discharge of industrial wastewater into receiving environments, which emphasizes the need of better wastewater treatment technologies (Heng et al., 2021). Especially, direct discharge of colored wastewater containing high amounts of organic pollutants, which is a typical scenario in industrial textile dyeing, causes toxicity and aesthetical pollution of natural water. Conventional methods such as biodegradation (Gurav et al., 2021; Sonwani et al., 2020), adsorption and filtration (Badawi and Zaher, 2021; Mansor et al., 2020), and coagulation-flocculation (Gökkuş et al., 2012; Mukhlish et al., 2020) are preferred for textile wastewater treatment, but present low treatment efficiency, high operation cost, or secondary pollution from accumulated sludge (Othmani et al., 2017; Titchou et al., 2021).

The electrochemical advanced oxidation processes (EAOPs) allow building up highly effective wastewater treatments able to achieve the complete pollutant mineralization (Sirés and Brillas, 2021). They include electrochemical oxidation (EO), electro-Fenton (EF), and photoelectro-Fenton (PEF) as main technologies (Tirado et al., 2018; Benekos et al., 2021). The EAOPs are based on the in-situ production of highly reactive oxidants such as hydroxyl radical ($^{\bullet}OH$) and sulfate radical ($SO_4^{\bullet-}$), which show a much higher oxidation potential than that of conventional oxidants such as chlorine (Cl_2), hydrogen peroxide (H_2O_2), or ozone (O_3) (Cornejo et al., 2021).

In all these EAOPs, physisorbed $^{\bullet}OH$ is formed at the anode (M) surface from water discharge (reaction (1)), yielding M($^{\bullet}OH$) as main oxidant in EO. The oxidation power in EF is comparatively enhanced due to the great production of free $^{\bullet}OH$ from Fenton's reaction (2) between added Fe^{2+} and generated H_2O_2, needed at lower concentrations as compared to conventional Fenton process. H_2O_2 is formed via cathodic reduction of injected O_2 from reaction (3) (Gökkuş and Yıldız, 2016; Thiam et al., 2018; Ren et al., 2023). In PEF, the solution is irradiated with UVA light to produce more $^{\bullet}OH$ from the photolysis of dissolved $[FeOH]^{2+}$ species via photo-Fenton reaction (4). Additionally, the final Fe(III)-carboxylate complexes can be rapidly photolyzed, enhancing the mineralization.

$$M + H_2O \rightarrow M(\dot{O}H) + H^+ + e^- \quad (1)$$

$$Fe^{2+} + H_2O_2 \rightarrow Fe^{3+} + \dot{O}H + OH^- \quad (2)$$

$$O_2 + 2H^+ + 2e^- \rightarrow H_2O_2 \quad (3)$$

$$[FeOH]^{2+} + h\nu \rightarrow Fe^{2+} + \dot{O}H \quad (4)$$

Electrocoagulation (EC) is another electrochemical method for the removal of recalcitrant and non-biodegradable pollutants. It takes place in three stages: (i) dissolution of the soluble anodes (iron or aluminum) through an electrical current (*I*); (ii) destabilization of the negatively charged pollutants, and (iii) removal of the destabilized flocs from the solution by flotation or precipitation. Fe anode can be dissolved to Fe^{2+} from reaction (5), which is transformed into insoluble $Fe(OH)_3$ in the presence of dissolved O_2 gas from the overall reaction (6). In parallel, OH^- ions and H_2 gas are released at the cathode surface from reaction (7) (Bruguera-Casamada et al., 2019).

$$Fe \rightarrow Fe^{2+} + 2e^- \quad (5)$$

$$4Fe + 10H_2O + O_{2(g)} \rightarrow 4Fe(OH)_{3(s)} + 4H_{2(g)} \quad (6)$$

$$2H_2O + 2e^- \rightarrow 2OH^- + H_{2(g)} \quad (7)$$

Many textile dyes such as C.I. Acid Red 336 (Sakthisharmila et al., 2018), C.I. Acid Orange 5 (Shokri, 2019), C.I. Acid Violet 17 (Pathak et al., 2021), C.I. Acid Green 20 (Moneer et al., 2021), C.I. Acid Red 18 (Shabestar et al., 2021) and C.I. Acid Brown 14 (AB14) diazo dye (Parsa et al., 2011; Bassyouni et al., 2017) have been subjected to EC treatment in batch systems. Significant advantages have been reported by combining the reaction and separation processes in continuous mode (Jiang et al., 2019; Thakur et al., 2019). Continuous-flow EC reactors with iron electrodes have also been tested for real indigo dyeing effluent (Hendaoui et al., 2018). The hybrid EC-EF process (i.e., 1-step treatment) has been successfully used to treat real textile wastewater (Louhichi et al., 2022; Xiao et al., 2022) and Remazol Black B dye solutions (Suhan et al., 2020). It is possible to reach complete mineralization in hybrid EC-EF systems, under different configurations such as electrochemical peroxidation (Gholikandi and Kazemirad, 2018; Suhan et al., 2020), peroxi-coagulation (Rao et al., 2022) or Fered-Fenton (Chen et al., 2023), but the long treatment time needed increases the cost significantly. The sequential EC-EF and EC-PEF treatments with batch systems in each step can also largely degrade recalcitrant contaminants, but a low H_2O_2 electrogeneration from reaction (3) may lead to electrode passivation during EF treatment (Nidheesh et al., 2021). An alternative to enhance the removal efficiency of these combined systems could be the use of a continuous-flow reactor in EC followed by EF or PEF treatments, as hypothesized by us in previous works (Flores et al., 2018; Ye et al., 2019). We present herein the novel operation of EC-EF in a scalable continuous-flow prototype, which has not been previously reported, to treat dye solutions.

This study aims to assess the performance of EC with a continuous-flow reactor with Fe electrodes to remove AB14 dye from aqueous solutions. A content of 50 mg L^{-1} of TOC was chosen for this dye, a typical content in textile industry wastewater (Yaseen and Scholz, 2019). EC was employed either as single treatment or as pre-treatment combined with EF and PEF processes. Both EAOPs were carried out in a recirculation system that included a one-compartment filter-press reactor equipped with a Pt anode and a carbon-PTFE air-diffusion cathode for H_2O_2 generation. The effect of the system configuration, electrolyte composition, pH, *I*, and liquid flow rate on the EC performance, as well as that of Fe^{2+} content in the Fenton-based EAOPs, was examined to optimize the treatment of the dyestuff solutions.

2. Materials and methods

2.1. Reagents

Commercial AB14 (purity >75 %, determined from total organic carbon (TOC) analysis) was supplied by Tokyo Chemical Industry and used as received. Reagent grade ferrous sulfate heptahydrate (> 98 %), sodium sulfate, sodium chloride, sodium hydrogen carbonate, sulfuric acid, and hydrochloric acid were purchased from Panreac, J.T. Baker and Merck. Analytical solutions were prepared with Millipore Milli-Q water (resistivity >18.2 MΩ cm), whereas the dye solutions were prepared with deionized water. Organic solvents and other chemicals were of analytical or HPLC grade purchased from Merck, Panreac, and Sigma-Aldrich.

2.2. Electrolytic systems

A scheme of the continuous-flow system used for the EC treatment of AB14 solutions is shown in Fig. 1a. The wastewater was injected by a magnetic pump into a purpose-made open and cylindrical acrylic reactor of 3 L capacity, operating at different liquid flow rates between 10 and

50 L h^{-1}. In some assays, compressed air was bubbled into the reactor at a flow rate of 1 L h^{-1} to (i) increase the oxidation of generated Fe^{2+} ions, thereby accelerating floc formation from reaction (6), and (ii) enhance the convection of the pollutants and electrolyte towards the anodes for their faster oxidation. The electrodes were Fe rods of 35.0 cm height and 1.0 cm diameter (~ 110 cm^2 area) each, which were distributed in a concentric configuration by inserting them in openings made in the top side of the reactor, with an inter-electrode gap of 1 cm. Fig. 1b highlights the five monopolar configurations with a different number of anodes (A) and cathodes (C): (i) 1A + 1C, (ii) 1A + 2C, (iii) 1A + 4C, (iv) 2A + 2C and (v) 5A + 4C. Before first use, all the electrodes were mechanically abraded using a SiC paper to remove the oxide surface layer, followed by acid washing with 0.1 M H_2SO_4 and rinsing with Milli-Q water. The EC trials were carried out at constant *I* using an Agilent 6552 A digital DC power supply, which directly displayed the cell voltage (E_{cell}). The runs were made in duplicate and the effect of the electrode configuration, electrolyte composition (NaCl, Na_2SO_4 or $NaHCO_3$), pH, *I*, liquid flow rate, and aeration on the treatment performance was studied.

Worth mentioning, the optimization sequence established for the EC process considers: (i) first, the optimization of the reactor type/configuration, in this case through the investigation of the effect of the number of electrodes; this gave rise to a system that was shown superior and hence, it served as the platform further employed for the rest of electrolytic trials; (ii) once optimized the reactor, the aqueous matrix (electrolyte and pH) had to be optimized, since several components could be investigated to mimic potentially real effluents entering the EC reactor; (iii) once confirmed the reactor and medium, the optimization of the operation variables was carried out; the effect of these variables on the process performance was expected to become gradually less important in order: current or flow rate, and aeration to conclude.

The sequential EC-EF and EC-PEF treatments were performed by coupling the previous EC reactor to the pre-pilot flow plant schematized in Fig. 2. That plant comprised a one-compartment electrochemical filter-press reactor equipped with a Pt anode and a carbon-PTFE air-diffusion cathode, both with an exposed surface area of 20 cm^2 and separated about 1 cm. The gas-diffusion cathode was fed with compressed air pumped at an overpressure of 8.6 kPa for continuous H_2O_2 production. An EC-treated solution of 2.5 L placed in the plant reservoir was recirculated through the electrochemical cell by means of a magnetic pump, at a fixed liquid flow rate of 180 L h^{-1} that was adjusted by a flowmeter. The solution temperature was regulated with water at 25 °C by two heat exchangers connected to a water bath. Worth noting, prior to coupling between EC and EF or PEF, the EC-treated solutions were filtered with paper filter and adjusted to pH 3.0 with sulfuric or hydrochloric acid (when the EC was made in sulfate and chloride media, respectively). This pH was chosen because it is optimal for the EF and PEF treatments of organic pollutants (Titchou et al., 2021; Ren et al., 2023). In the plant, the outlet of the electrochemical cell was connected to an annular glass photoreactor of 640 mL volume, whose outlet was connected to the reservoir. The photoreactor was covered with an opaque cloth in EF, whereas it contained an E27 125-W UVA lamp (320–400 nm, λ_{max} = 360 nm) from Omnilux to irradiate the solution in PEF trials. The irradiance of this lamp was 105 W m^{-2}, as measured with a Kipp & Zonen CUV 5 radiometer. The Fenton-based assays were made in duplicate by applying a constant *I* provided by a Grelco GVD310 DC power supply, which allowed the monitoring of E_{cell}.

2.3. Analytical methods

The solution pH and specific conductivity were monitored with a GLP 22 pH meter from Crison and a Methrom 644 conductometer. The titanium sulfate colorimetric method served to determine the H_2O_2 concentration on a Shimadzu 1800 UV/Vis spectrophotometer set at λ = 408 nm and thermostated at 25 °C (Welcher, 1975). Before analysis of the EC samples, they were filtered with 0.45 mm PTFE syringe filters from Whatman. In the Fenton-based processes, immediately after sample collection their pH was adjusted to pH 8.0 to stop the degradation process, and then filtered with the above filters prior to their analysis.

The λ_{max} of the UV/Vis spectrum of AB14 solutions depended on their pH (see the chemical structure and physicochemical properties of the dye in Table S1). Preliminary assays showed a peak at λ_{max} values of 453, 462 and 497 nm at pH values of 3.0, 8.0–10.0 and 12.0,

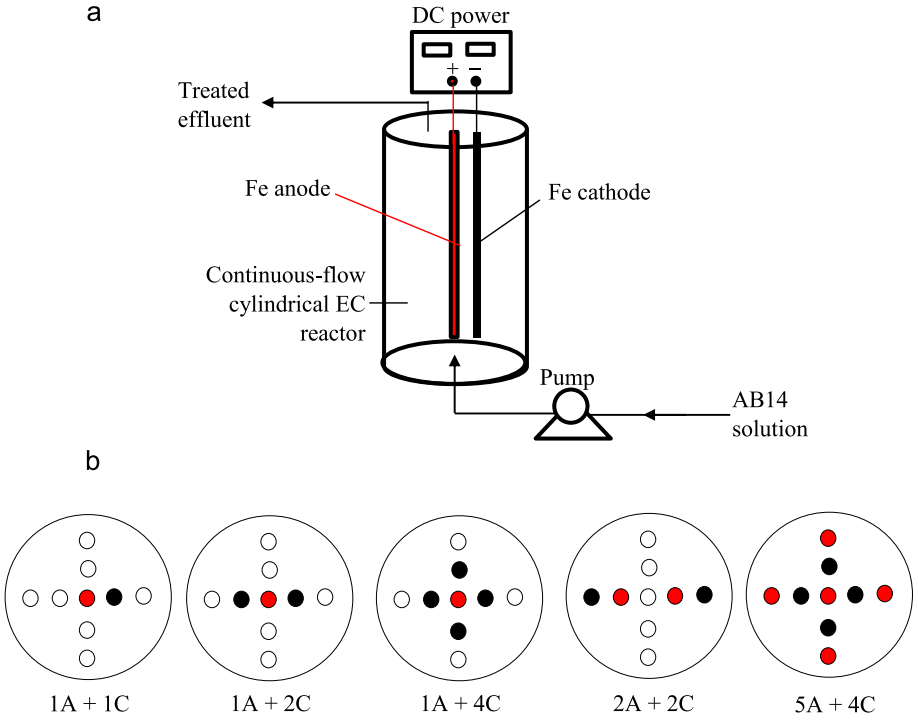

Fig. 1. (a) Scheme of the experimental setup used for the EC treatment of AB14 solutions in continuous mode with 1 Fe anode and 1 Fe cathode. (b) Top view of the EC reactor showing the electrode configurations used. ● = Anode (A), ● = cathode (C).

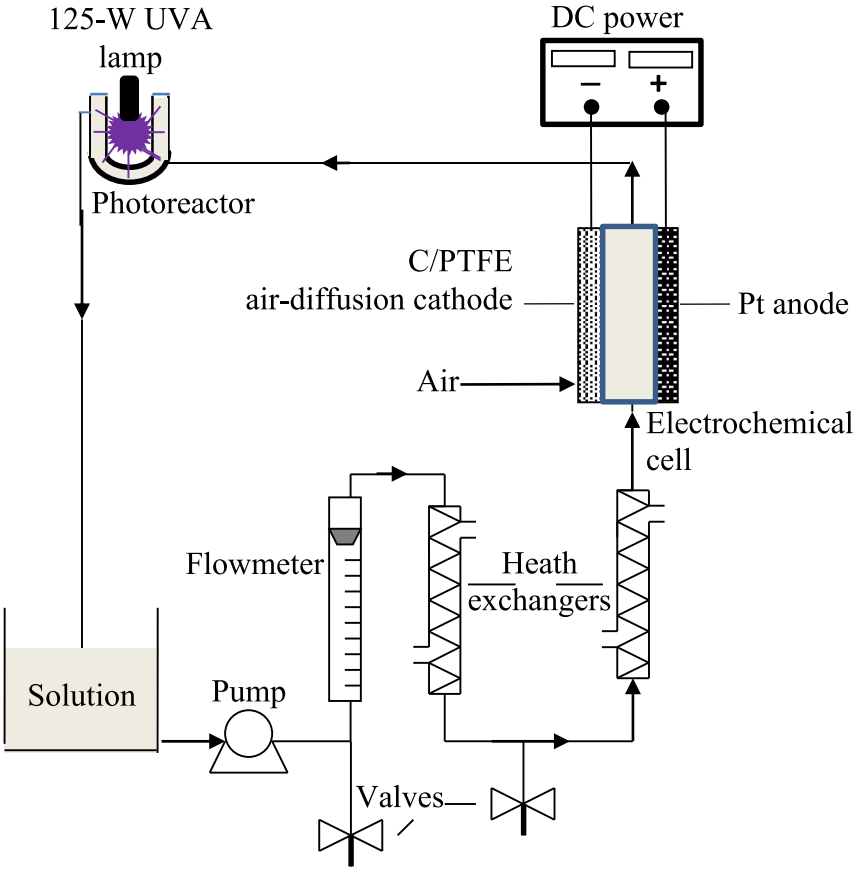

Fig. 2. Sketch of the pre-pilot flow plant used for the EF or PEF treatments performed after the EC treatment of AB14 solutions. In EF, the lamp was switch off and the photoreactor was covered with an opaque cloth.

respectively, at 25 °C. The absorbance (A) was then determined at the corresponding λ_{max} of the treated solution using the above spectrophotometer, kept at 25 °C. The percentage of color removal from an initial absorbance A_0 could be calculated from Eq. (8) (Thiam et al., 2015).

$$\%\text{Color removal} = \frac{A_o - A}{A_o}\ 100 \tag{8}$$

The solution TOC was determined with a Shimadzu VCSN TOC analyzer using the non-purgeable organic carbon (NPOC) method. Results with a deviation as low as ±1 % were obtained upon injection of 50 μL aliquots into the analyzer. From these results, the percentage of TOC removal was calculated from the initial TOC (i.e., TOC_0) and the TOC at a given treatment time, as follows:

$$\%\text{TOC removal} = \frac{TOC_o - TOC}{TOC_o}\ 100 \tag{9}$$

For the EC process under steady conditions, the energy consumption per gram of TOC (EC_{TOC}, in kWh (g TOC)$^{-1}$) and the corresponding energy consumption per cubic meter (EC_V, in kWh m^{-3}) were calculated from Eqs. (10) and (11):

$$EC_{TOC} = \frac{E_{cell}\ I}{LFR\ \Delta TOC} \tag{10}$$

$$EC_V = \frac{E_{cell}\ I}{LFR} \tag{11}$$

where E_{cell} is given in V and the current I in A. ΔTOC accounts for the TOC abatement, in mg L^{-1}, and the liquid flow rate (LFR) is in L h^{-1}. This latter parameter was calculated as the ratio between the EC reactor capacity (3 L) and its hydraulic retention time (HRT) in h. In the case of EF and PEF treatments, such energy consumptions at a given time t (in h) were determined from Eqs. (12) and (13), respectively:

$$EC_{TOC} = \frac{E_{cell}\ I\ t}{V\Delta TOC} \tag{12}$$

$$EC_V = \frac{E_{cell}\ I\ t}{V} \tag{13}$$

In the case of PEF, the corresponding total energy consumptions, $EC_{TOC,total}$ and $EC_{V,total}$, included the energy consumed by the 125-W UVA lamp, according to Eqs. (14) and (15):

$$EC_{TOC,total} = \frac{(E_{cell}\ I + 125)t}{V\Delta TOC} \tag{14}$$

$$EC_{V,total} = \frac{(E_{cell}\ I + 125)t}{V} \tag{15}$$

The terms EC_{TOC}, EC_V, $EC_{TOC,total}$ and $EC_{V,total}$ were also used to determine the sum of the energy consumption of the sequential EC-EF and EC-PEF processes.

The concentration of metal cations was obtained by inductively coupled plasma-optical emission spectroscopy (IPC-OES) with a Perkin Elmer Optima 3200 L spectrometer. The concentration of Cl^-, ClO_3^-, ClO_4^-, $NO_3^-$and SO_4^{2-} ions was determined by ion chromatography upon injection of 20 μL samples into a Kontron 465 liquid chromatograph, fitted with a Waters IC-Pack (4.6 mm × 150 mm) anion column at 35 °C, and coupled with a Waters 432 conductivity detector. The mobile phase for this analysis was a solution established by EPA 9056, and it was eluted at 2 mL min^{-1}.

3. Results and discussion

This section presents the results obtained for EC in continuous mode, as well as the sequential EC-EF and EC-PEF treatments of AB14 solutions. The change in removal efficiencies of EC process was evaluated with and without compressed air bubbling into the continuous-flow EC reactor. First, an AB14 dye solution with 50 mg L^{-1} TOC was treated in the EC reactor to optimize the operation conditions. The optimized EC was then coupled with EF and PEF processes to evaluate the overall color and TOC removals.

3.1. EC treatment in a continuous-flow reactor

3.1.1. Effect of the number of electrodes

Table 1 summarizes the detailed experimental conditions and results obtained during the optimization of the EC treatment of AB14 dye solutions with 50 mg L^{-1} TOC. First, the electrode configuration, i.e., the number of Fe anodes and cathodes used, was considered. Fig. 3 shows the color and TOC removal efficiencies at liquid flow rate of 10 L h^{-1} using different electrode configurations, as well as different applied I to control the current density (j). The number of electrodes used in the EC process affects the pollutant removal efficiency, since a higher number leads to a higher energy consumption and larger generation of flocs in a shorter time (Malakootian et al., 2011). As can be seen in Fig. 3a, a high percentage of color removal around 70 % (between 66.8 % and 70.7 %) was found using one Fe anode and several cathodes in 39.6 mM NaCl medium at $I = 2.19$ A. However, very low TOC removals were attained, decreasing from 3.1 % to 0.2 % when rising from 1 to 4 cathodes. Fig. 3b shows the change of the same parameters employing 1A + 1C, 2A + 2C and 5A + 4C configurations, at increasing I values from 2.19 to 10.15 A to ensure a constant anodic current density around 20 mA cm^{-2} in all cases. While the 1A + 1C arrangement yielded 66.8 % color and 3.1 % TOC abatements with $EC_V = 1.97$ kWh m^{-3}, enhanced color and TOC removals (i.e., 98.1 % and 20.1 %, respectively) were obtained for the best electrode configuration of 5A + 4C, with $EC_V = 6.90$ kWh m^{-3} (see Table 1). Worse behavior was found for the 2A + 2C configuration, reaching the same color removal but with a smaller TOC decay (i.e., 19.3 %) and higher $EC_V = 2.64$ kWh m^{-3} (see Table 1). The direct relationship between the higher number of anodes and the better removal efficiency can be explained by the increase in the total anode surface area. This originated a greater amount of coagulant added to the solution, giving rise to a quicker coagulation of the dye molecules (Mousazadeh et al., 2021). These tendencies agree with those reported in a work using an EC reactor containing Al plates for the removal of Cu, Cr and Ni ions from a metal plating industry wastewater, operating in batch mode for 10 min; the authors found that the increase of the number of Al anodes, from two to six, enhanced the percentages of Cu, Cr and Ni abatements from 77.8 % to 97.5 %, 71.9 % to 93.2 % and 40.2 % to 74.1 %, respectively (Akbal and Camcı, 2011).

From the above findings, one can conclude that the 5A + 4C configuration is superior, leading to almost total decolorization but with a low TOC removal. All subsequent EC assays were carried out using this optimum configuration.

Table 1
Results obtained for the EC treatment of solutions containing 50 mg L^{-1} TOC of AB14 in a continuous-flow reactor of 3 L capacity under different experimental conditions.

Electrode configuration	Medium	Liquid flow rate ($L\ h^{-1}$)	I (A)	E_{cell} (V)	pH initial (steady)	Conductivity (mS cm^{-1}) initial (steady)	% Color removal	% TOC removal	EC_{TOC} (kWh (g TOC)$^{-1}$)	EC_V (kWh m^{-3})
1A + 1C	39.6 mM NaCl	10	2.19	9.0	7.9 (10.6)	2.47 (2.67)	66.8	3.12	1.243	1.97
1A + 2C	39.6 mM NaCl	10	2.19	6.3	7.7 (10.6)	3.18 (3.29)	70.7	2.11	1.308	1.38
1A + 4C	39.6 mM NaCl	10	2.19	5.2	7.5 (10.1)	3.25 (3.37)	67.1	0.17	13.65	1.14
2A + 2C	39.6 mM NaCl	10	2.19	3.8	8.9 (10.0)	2.28 (2.43)	71.9	17.8	0.093	0.83
	39.6 mM NaCl	10	4.40	6.0	8.4 (10.4)	2.43 (2.63)	98.3	19.3	0.273	2.64
	39.6 mM NaCl	10	6.57	8.5	8.2 (10.7)	2.51 (2.78)	93.5	58.0	0.192	5.58
	20 mM Na_2SO_4	10	2.19	4.2	8.3 (–[b])	- [b]	68.2	- [b]	- [b]	0.92
	20 mM Na_2SO_4	20	2.19	4.8	8.4 (10.1)	2.35 (2.51)	27.1	9.56	0.110	0.53
	20 mM Na_2SO_4	30	2.19	4.5	8.3 (9.4)	2.35 (2.51)	9.31	- [b]	- [b]	0.33
	54.6 mM $NaHCO_3$	10	2.19	10.2	8.3 (8.7)	2.36 (2.43)	11.7	9.40	0.475	2.23
5A + 4C	39.6 mM NaCl	10	8.21	5.0	7.9 (10.9)	3.72 (3.82)	98.1	13.0	0.631	5.17
	39.6 mM NaCl	10	10.95	6.1	4.0 (11.0)	3.58 (3.84)	99.7	18.6	0.717	6.68
	39.6 mM NaCl	10	10.95	6.3	7.6 (10.9)	3.21 (3.49)	98.1	20.1	0.685	6.90
	39.6 mM NaCl +air supply	10	10.95	6.6	6.9 (10.9)	3.24 (3.55)	99.6	31.7	0.456	7.23
	39.6 mM NaCl	10	10.95	6.4	10.0 (11.0)	3.58 (3.89)	98.1	21.8	0.642	7.00
	39.6 mM NaCl	10	10.95	6.2	12.0 (11.9)	4.42 (4.84)	95.3	13.6	1.009	6.79
	39.6 mM NaCl	10	13.70	7.6	4.0 (10.8)	3.73 (4.17)	96.0	26.2	0.794	10.41
	39.6 mM NaCl +air supply	10	13.70	8.0	4.0 (11.1)	3.21 (3.51)	99.5	31.5	0.696	10.96
	39.6 mM NaCl	10	13.70	7.6	7.8 (10.8)	3.82 (3.91)	96.8	23.3	0.892	10.41
	39.6 mM NaCl +air supply	10	13.70	8.6	7.0 (10.9)	3.01 (3.30)	99.6	32.1	0.733	9.42
	39.6 mM NaCl	25	10.95	6.8	8.0 (10.9)	3.37 (3.68)	98.4	20.8	0.895	9.32
	39.6 mM NaCl	50	10.95	6.9	7.9 (10.7)	3.37 (3.52)	98.7	14.1	1.347	9.45
	20 mM Na_2SO_4	10	10.95	7.4	6.3 (11.1)	3.51 (3.77)	98.5	19.1	0.847	8.10
	20 mM Na_2SO_4 +air supply	10	10.95	8.7	7.0 (10.7)	3.51 (3.77)	97.9	18.4	1.038	9.53
	20 mM Na_2SO_4	10	13.70	9.1	7.7 (11.3)	3.04 (3.45)	97.7	23.5	1.061	12.47
	20 mM Na_2SO_4 +air supply	10	13.70	10.9	7.2 (11.2)	2.92 (3.20)	94.6	21.5	1.388	14.93
	54.6 mM $NaHCO_3$	10	10.95	11.6	8.2 (8.8)	3.37 (3.47)	14.1	13.5	1.882	12.70
	Mixture [a]	10	10.95	7.1	8.3 (9.5)	3.42 (3.58)	94.5	17.6	0.883	7.77
	Mixture [a] +air supply	10	10.95	9.9	8.3 (9.8)	3.24 (3.40)	93.6	13.4	1.617	10.84

[a] 6.7 mM Na_2SO_4 + 13.2 mM NaCl +18.2 mM $NaHCO_3$.
[b] Not determined.

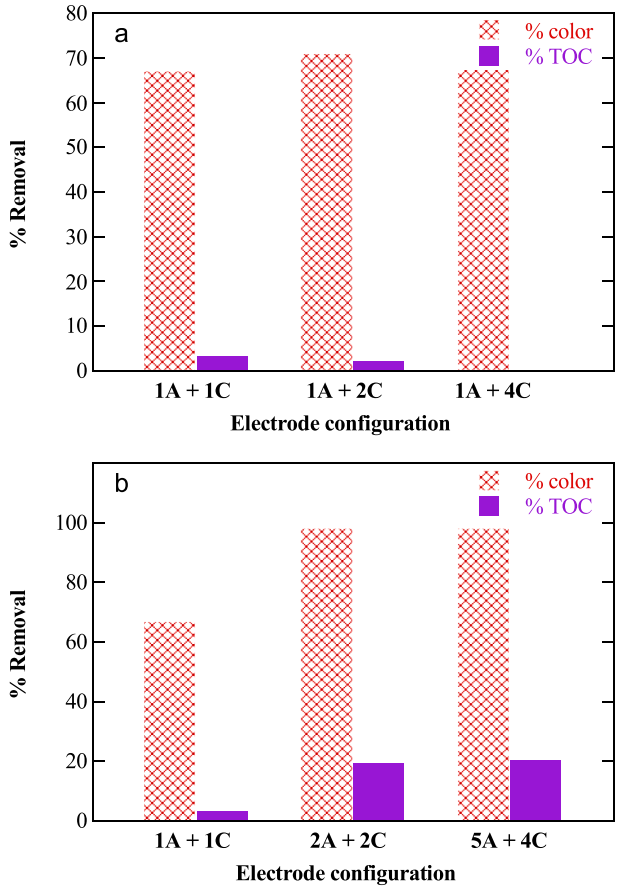

Fig. 3. Variation of the percentage of color and TOC removals with (a) the number of Fe cathodes (connected to 1 Fe anode) and (b) the number of Fe anodes for the EC treatment of 50 mg L^{-1} TOC of AB14 in 39.6 mM NaCl medium at natural pH and liquid flow rate of 10 L h^{-1}, once reached the steady-state conditions using the continuous-flow reactor of Fig. 1. In (a), current (I) = 2.19 A. In (b), I = 2.19, 4.40 and 10.95 A for the 1A + 1C, 2A + 2C and 5A + 4C configurations, respectively. In all the assays, the anodic current density was ~20 mA cm^{-2}.

3.1.2. *Effect of background electrolyte*

The electrolyte composition can directly affect the metal dissolution rate and the energy consumption by increasing/reducing the cell voltage. Moreover, it has been shown that the electrolyte nature could significantly influence the behavior of the bubble generation at the electrodes, thus affecting the agglomeration and dissemination of the produced flocs (Keyikoglu et al., 2019). Fig. 4a depicts the color and TOC removal profiles obtained during the continuous-flow EC experiments with three types of background electrolytes ($NaSO_4$, NaCl and $NaHCO_3$) using the 5A + 4C electrode configuration. Concentrations of 20 mM, 39.6 mM and 54.6 mM were used for $NaSO_4$, NaCl and $NaHCO_3$, respectively, in order to ensure that the solutions had the same conductivity (approximately 2.39 mS cm^{-1}). As can be seen in Fig. 4a, the effectiveness for removing the AB14 dye was greatly dependent on the electrolyte, increasing in the order $NaHCO_3 < Na_2SO_4 <$ NaCl as shown by the gradually greater decolorization and TOC removal efficiencies of 14.1–13.5 %, 98.5–19.1 % and 98.1–20.1 %, respectively. The calculated EC_V values decreased from 12.70 to 8.10 and 6.90 kWh m^{-3}, respectively (see Table 1). The superiority evidenced in chloride medium can be explained by the formation of oxidants like active chlorine, whose speciation (Cl_2/HClO/ClO^- species) depends on the solution pH, from Cl^- oxidation at the anode following reaction (16) and the subsequent hydrolysis in the bulk according to reactions (17) and (18) (Yıldız et al., 2008).

$$2Cl^- \rightarrow Cl_2 + 2e^- \quad (16)$$

$$Cl_2 + H_2O \rightarrow HOCl + Cl^- + H^+ \quad (17)$$

$$HOCl \leftrightarrow ClO^- + H^+ \; pK_a = 7.55 \quad (18)$$

However, note that both NaCl and $NaSO_4$ electrolytes yielded close results, which means that actually the production of active chlorine at the sacrificial Fe anode is low and the main oxidant is $^{\bullet}OH$ in both cases. Therefore, one can infer that the mechanism of the EC process involves: (i) the coagulation of organic molecules containing chromophore groups induced by the insoluble $Fe(OH)_3$, which can explain the overall color removal but not the partial TOC abatement; and (ii) the action of oxidants like $^{\bullet}OH$ (and active chlorine to a smaller extent) on organics, originating colorless by-products from the dye cleavage such as benzenic and naphthalenic derivatives and carboxylic acids that account for the residual TOC.

The study of the influence of the electrolyte on the removal of AB14 was extended to a mixture of salts trying to simulate typical conditions in textile industry wastewater. To do this, a solution with 50 mg L^{-1} of TOC of the dye in a 6.7 mM Na_2SO_4 + 13.2 mM NaCl +18.2 mM $NaHCO_3$ mixture, showing the same conductivity as that the above single electrolytes, was treatment by EC under the 5A + 4C configuration at I = 7.1 A, natural pH and liquid flow rate of 10 L h^{-1}. Under these conditions, the results of Table 1 show that 95.4 % of color removal and 17.7 % of TOC abatement were obtained, with an EC_V value of 7.77 kWh m^{-3}. If compared with the best results obtained before, in 39.6 mM NaCl, a loss of 3.3 % in color removal and 2.4 % in TOC reduction, with a rise of 0.87 kWh m^{-3} in EC_V, is found in the mixed electrolyte. The presence of SO_4^{2-} and, mainly, HCO_3^-, in the mixture may reduce the performance of the EC process because these anions: (i) can form a passive layer on the metal surface or thicken the existing one, and (ii) can become adsorbed on the anode surface, thus inhibiting the dye adsorption or blocking some active sties (Maitlo et al., 2019).

Based on these results, further assays with the continuous-flow EC system were performed in NaCl medium, since it showed the best performance in terms of TOC removal thanks to the oxidation of organics with active chlorine.

3.1.3. *Effect of initial pH*

The solution pH is a key parameter in the EC process because it affects the concentration of the metal dissolved from the Fe anode, thus being responsible for the formation of the flocs to adsorb the dye (Simon et al., 2023). To examine the effect of pH on the performance of the continuous-flow EC process, a series of trials was made by treating the dye solution of 50 mg L^{-1} TOC in 39.6 mM NaCl at pH 4.0, 7.6 (natural pH), 10.0 and 12.0, at I = 10.95 A and liquid flow rate of 10 L h^{-1}. Fig. 4b illustrates the results obtained for these assays. A color removal >98 % can be observed in the pH interval of 4.0–10.0, which decayed to 95 % at pH 12.0. The same tendency was found for the TOC abatement, with values near 20 % in the above interval that decayed to 13 % at the most alkaline pH. The highest TOC removal efficiency of 21.8 % was obtained at pH 10.0, corresponding to EC_V = 7.0 kWh m^{-3}. A change in the performance of the EC process with pH is expected, depending on the nature of the contaminants, although usually the EC with iron electrodes is superior at alkaline pH. Note also that the spontaneous dissolution of iron electrodes occurs at acidic pH in the absence of applied I, whereas such phenomenon is less significant at higher pH (Mousazadeh et al., 2021). The final pH determined for the trials of Fig. 4b in the range from 4.0 to 10.0 was ca. 11.0, whereas it was 11.9 when the initial pH was 12.0 (see Table 1). This means that practically no iron was dissolved from the electrodes starting at pH = 4.0. The formation of OH^- ions at the cathode during the electrolysis, according to reaction (7), can explain the strong alkalinization of the solutions at initial pH ≤ 10.0 (Mousazadeh et al., 2021). This pH convergence suggests the formation of a similar number of flocs in trials starting at pH 4.0–10.0, ending in

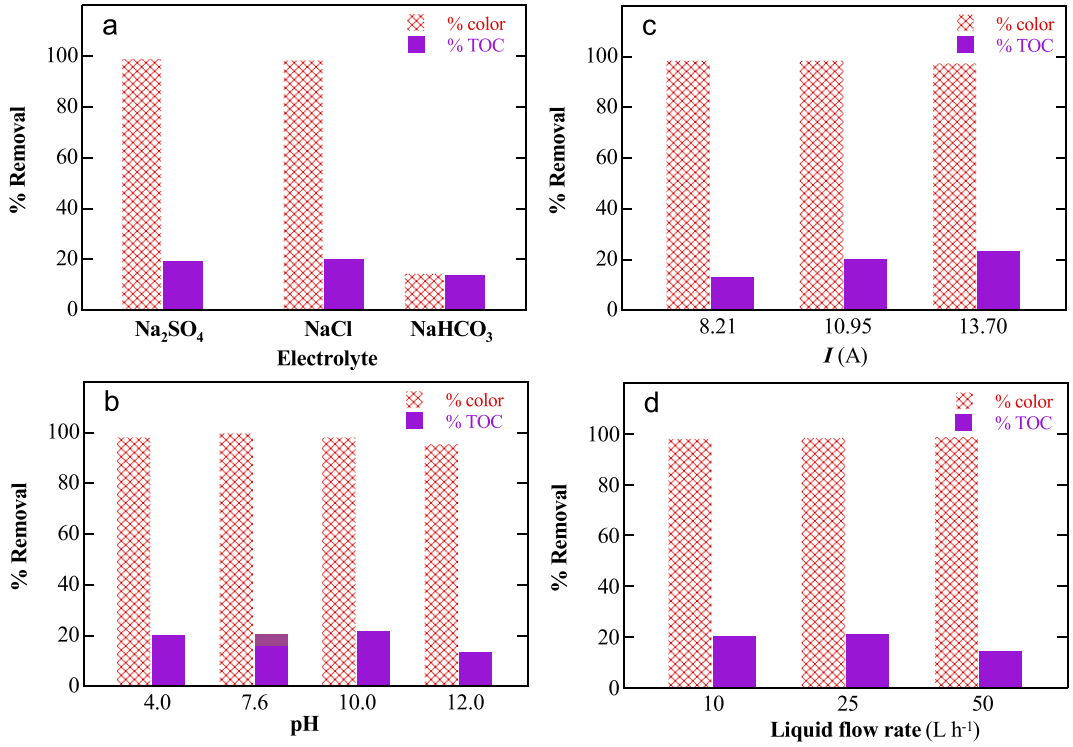

Fig. 4. Variation of the percentage of color and TOC removals for the EC treatment of 50 mg L^{-1} TOC of AB14, once reached the steady-state conditions using the continuous-flow reactor of Fig. 1 with the 5A + 4C configuration. Effect of: (a) Electrolyte, employing 20 mM Na_2SO_4, 39.6 mM NaCl or 54.6 mM $NaHCO_3$ solutions at natural pH, liquid flow rate of 10 L h^{-1} and I = 10.95 A; (b) applied current (corresponding to increasing anodic current densities of ~15, 20 and 25 mA cm^{-2}), using 39.6 mM NaCl medium at natural pH and liquid flow rate of 10 L h^{-1}; (c) pH, employing 39.6 mM NaCl medium, liquid flow rate of 10 L h^{-1} and I = 10.95 A; and (d) liquid flow rate, using 39.6 mM NaCl medium at natural pH and I = 10.95 A.

similar removals of AB14, whereas a lower number of flocs led to a poorer adsorption of organics in the trial at pH 12.0. This agrees with the work of İrdemez et al. (2006), who stated that low pH values are more suitable for the formation of insoluble iron hydroxide compounds in the EC treatment with iron electrodes. In contrast, at high pH values, both insoluble $Fe(OH)_3$ and soluble $Fe(OH)_4^-$ are present in the medium, decreasing the action of the generated flocs over the organic pollutants. This can be confirmed from the predominance-zone diagrams for Fe(III) chemical species in aqueous solution presented in Fig. S1.

In view of these findings, revealing the best performance in the pH range 4.0–10.0, natural pH 7.6 was used in further trials because it is the value expected for industrial dye wastewater.

3.1.4. Effect of applied current

The applied current not only determines the coagulant dose rate, but also the bubble production rate and size, and all these factors eventually affect the EC efficiency (Thiam et al., 2014). According to Faraday's law, the dissolution of the anode increases at a higher current, thus producing more ions and hence, more flocs that trap the dye and its by-products (Thiam et al., 2014). This behavior can be seen in Fig. 4c, which depicts the color and TOC removals found for the 50 mg L^{-1} TOC solution in 39.6 mM NaCl at natural pH when values of 8.21, 10.95 and 13.70 A (i.e., anodic current density of ~15, 20 and 25 mA cm^{-2}) were applied using the 5A + 4C configuration. A color removal efficiency of over 96 % can be observed regardless of the applied I. The best color removal efficiency of 98.1 % was found at I values of 8.21 and 10.95 A. Conversely, there are significant differences in terms of TOC removal efficiencies, showing a significant increase with increasing I. The TOC abatement almost doubled, from 13 % to 23 %, when I was risen from 8.21 to 13.70 A, meaning that the release of more Fe^{2+} removed more dye and its by-products by coagulation. This is probably due to the formation of flocs of larger size and area, which allowed a larger adsorption of organics on their surface. As expected, the energy consumption was also greater at higher I, with EC_V values of 5.17, 6.90 and 10.41 kWh m^{-3} at 8.21, 10.95 and 13.70 A, respectively. Despite this, the optimum current for EC treatment of AB14 solutions in continuous mode, in terms of TOC reduction, was 13.70 A. This current was then chosen for the subsequent optimization assays.

3.1.5. Effect of liquid flow rate

Several authors have reported that the increase of the liquid flow rate using a continuous-flow EC reactor is detrimental, since the color removal decreases due to the reduction of the metal ion concentration per unit of time and volume (Mollah et al., 2004; Zodi et al., 2013; Zampeta et al., 2022). To clarify the effect of liquid flow rate on color and TOC removals in our system, several trials were performed at LFR of 10, 25 and 50 L h^{-1} for the treatment of 50 mg L^{-1} TOC of AB14 in 39.6 mM NaCl at natural pH and I = 10.95 A. Fig. 4d shows that 98 % decolorization with 14 % TOC reduction could be achieved at LFR = 50 L h^{-1}. A similar decolorization can be observed at 10 and 25 L h^{-1}, but with a much higher TOC removal of 20–21 % in both cases (see Table 1). In a continuous-flow EC system, the reduction of the liquid flow rate entails a larger HRT, allowing the iron hydroxide flocs to be restabilized. In other words, the rise of retention time limits the mixing in the reactor. The mixing affects the formation and growth of flocs inside the reactor, as well as their coagulation phenomena (Kobya et al., 2016). Therefore, the appropriate value of the liquid flow rate to attain the maximum removal performance is sensitive to reactor design. To assess this in our system, the EC_V values at the three LFR values were calculated, as can be seen in Table 1. When the flow rate was risen from 10 to 50 L h^{-1}, the EC_V value grew from 6.90 to 9.45 kWh m^{-3}, i.e., the energy consumption increased approximately 1.4 times.

The lowest LFR (i.e, 10 L h^{-1}) was selected because it yielded 98.1 % color decay and 20.1 % TOC removal with the lowest EC_V of 6.90 kWh

m^{-3}. This means that only 18 min were required to carry out the continuous-flow EC treatment.

3.1.6. Aeration of the continuous-flow EC reactor

The aeration with pure oxygen or air of a solution during its EC treatment with iron electrodes may enhance the treatment performance, as reported for the removal of arsenic (Dubrawski et al., 2015; Syam Babu et al., 2021), perfluorooctanoic acid (Singh et al., 2021), cyanide (Moussavi et al., 2011b), petroleum hydrocarbons from groundwater (Moussavi et al., 2011a), composite wastewater (Kumar et al., 2018), dairy industry wastewater (Akansha et al., 2020), and thallium from industrial wastewater (Fu et al., 2020). The performance achieved in an aerated EC process is the same as that of conventional EC until the dissolved oxygen in the solution is depleted. This occurs because the species mainly responsible for contaminant removal in the EC process is the insoluble ferric hydroxide, which needs O_2 for its production from reaction (6) (Nidheesh and Gökkuş, 2023). Fig. 5a-d depict the color and TOC removals attained for the treatment of AB14 dye solution with 50 mg L^{-1} TOC in the continuous-flow EC reactor, with aeration at 1 L h^{-1} and without air bubbling. Fig. 5a presents the positive effect of aeration on removal efficiency in 39.6 mM NaCl medium at neutral pH and I values of 10.95 and 13.70 A. At 10.95 A, the decolorization was increased from 98.1 % to 99.6 % and the TOC was reduced from 21.8 % to 31.7 % under aeration. In contrast, the EC_V for the non-aerated trial was 7.00 kWh m^{-3}, a smaller value than 7.23 kWh m^{-3} calculated with aeration (see Table 1). Similar trends were obtained at 13.70 A, with color and TOC decays rising from 96 % to 99.5 % and from 26.2 % to 31.5 %, respectively, under aeration, whereas the EC_V value increased from 10.41 to 10.96 kWh m^{-3}. Fig. 5b shows the corresponding results determined under the same conditions with 20 mM Na_2SO_4 as background electrolyte at natural pH. Unlike the behavior found in chloride medium, no significant effect of aeration can be observed in sulfate medium. These findings make evident that in our system, aeration does not affect the formation of flocs in the EC process from reaction (6) and hence, the positive effect of Cl^- can be related to the enhanced contribution of active chlorine as oxidant in this system (Tirado et al., 2018).

The performance of the continuous-flow EC in 39.6 mM NaCl medium was also explored at pH 4.0 under aeration. Fig. 5c shows a similar behavior to that of Fig. 5a obtained at neutral pH. Hence, under aeration, the color abatement was risen from 96 % to 99.5 %, and the TOC decay from 26.2 % to 31.5 %. Our results confirm that the aeration of the polluted solutions in chloride medium enhanced the removal efficiency of the EC process, as has also been reported by Nidheesh and Gökkuş, 2023. In contrast, this was not verified in a solution prepared in the 6.7 mM Na_2SO_4 + 13.2 mM NaCl +18.2 mM $NaHCO_3$ mixture. Fig. 5d reveals that the aeration worsened the performance, at natural pH and I = 10.95 A. Furthermore, a high EC_V = 14.93 kWh m^{-3} was found in the aerated trial, about 2.5 kWh m^{-3} higher than EC_V = 12.47 kWh m^{-3} determined without aeration. This means that the possible benefits of aeration must be assessed for each specific solution. It enhances the performance in chloride medium, but it has a negative impact in matrices with sulfate.

3.2. Sequential EC-EF and EC-PEF treatments

3.2.1. H_2O_2 electrogeneration in the pre-pilot flow plant

Fig. S2a shows the H_2O_2 accumulation with time in the pre-pilot plant of Fig. 2, corresponding to the treatment of 2.5 L of a 0.05 M Na_2SO_4 solution at pH 3.0, recirculated at a liquid flow rate of 180 L h^{-1}. H_2O_2 was formed upon O_2 reduction at the air-diffusion cathode at various j values ranging from 25 to 100 mA cm^{-2}, in the absence and presence of UVA irradiation. The accumulated H_2O_2 content always increased with time and with rising j, until a steady value was reached when its electrogeneration rate from reaction (3) became equal to its destruction one, pre-eminently due to its oxidation at the anode producing the weak oxidant hydroperoxyl radical ($HO_2^{\bullet}$) (Daniel et al.,

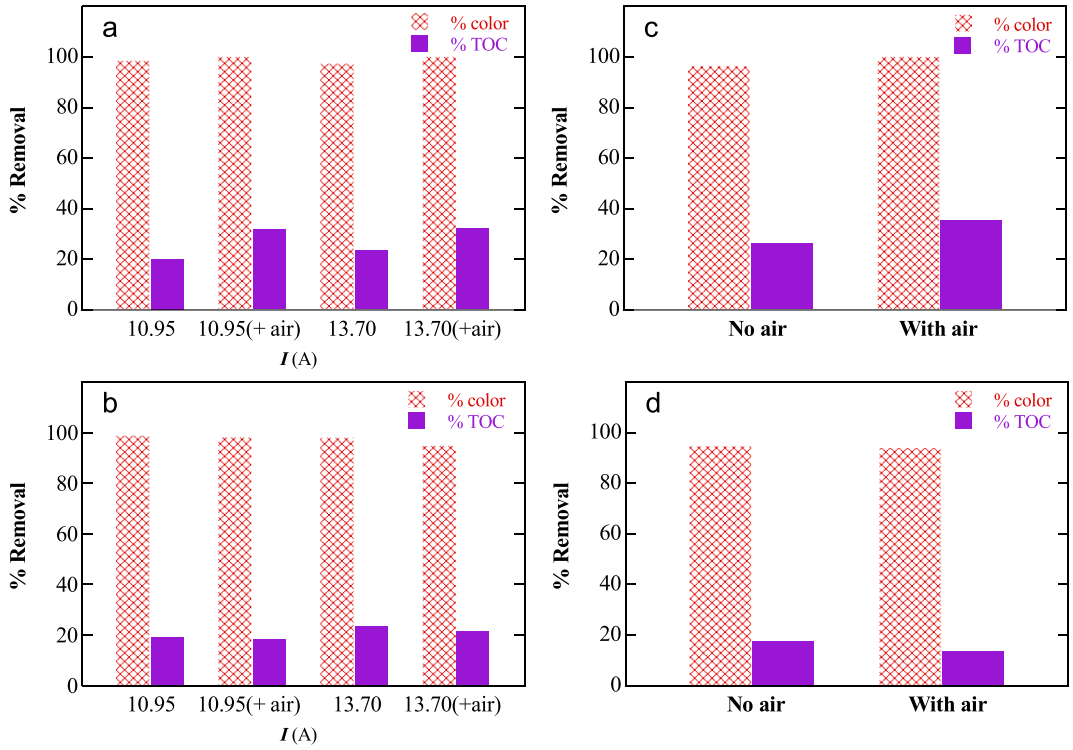

Fig. 5. Variation of the percentage of color and TOC removals for the EC treatment of 50 mg L^{-1} TOC of AB14 without and with O_2 (air bubbling at 1 L h^{-1}), once reached the steady-state conditions using the continuous-flow reactor of Fig. 1 with the 5 A + 4C configuration at a liquid flow rate of 10 L h^{-1}. Influence of current on removals: (a) 39.6 mM NaCl and (b) 20 mM Na_2SO_4 media, both at natural pH. Influence of air bubbling on removals: (c) 39.6 mM NaCl medium at pH 4.0 and I = 13.70 A; (d) 6.7 mM Na_2SO_4 + 13.2 mM NaCl +18.2 mM $NaHCO_3$ mixture at natural pH and I = 10.95 A.

2020).

Gradually lower maximum H_2O_2 concentrations of 1250, 925 and 456 mg L^{-1} as j values decreased from 100 to 50 and 25 mA cm^{-2}, respectively, were observed. Fig. S2b highlights the opposite profiles for the current efficiency (CE) for H_2O_2 accumulation, which was determined from Faraday's law. In all cases, CE decreased with time due to the continuous destruction of H_2O_2. For the most efficient process, occurring at the lowest $j = 25$ mA cm^{-2}, CE dropped from 17.4 % at the beginning of the electrolysis down to 6.8 % at 540 min. Final values of 6.7 % and 4.3 % were attained at 50 and 100 mA cm^{-2}, respectively.

Fig. S2a also shows the decrease of accumulated H_2O_2 when 0.50 mM Fe^{2+} was added to the sulfate solution at $j = 50$ mA cm^{-2} due to the consumption of this species from Fenton's reaction (2). A steady state with 242 mg L^{-1} H_2O_2 was achieved and the final CE value was 1.8 % (see Fig. S2b). The irradiation of the solution with the 125-W UVA lamp accelerated the H_2O_2 decomposition by the additional action of photo-Fenton reaction (4), reaching a concentration of 199 mg L^{-1} with a final CE = 1.5 % (see Fig. S2a and b). These results corroborate that our pre-pilot plant is able to produce enough H_2O_2 to generate $^{\bullet}OH$ from reactions (2) and (4), forecasting an effective destruction of organics.

3.2.2. *Sequential EC-EF treatment of AB14 solutions*

The above results with the continuous-flow EC reactor revealed that, although this treatment yielded good results for color removal, its TOC removal efficiency was very limited. The EC-treated (i.e., 15 min) effluents in 39.6 mM NaCl or 20 mM Na_2SO_4 media at neutral pH were subsequently treated by EF in the pre-pilot flow plant at $j = 50$ mA cm^{-2}. Fig. 6a and c depict the TOC concentration decay with electrolysis time in the EC-EF tests. The EF treatments were made with 2.5 L of the EC supernatant resulting at 15 min, after filtration, adjusting the pH to 3.0 and the addition of Fe^{2+} content between 0.10 and 1.0 mM. This catalytic Fe^{2+} was added in these EF processes because its analysis in the EC-treated solutions revealed residual values due to its practical overall conversion into $Fe(OH)_3$. In EF, the degradation of organics occurred by the attack of physisorbed Pt($^{\bullet}OH$) formed from reaction (1) when they arrived at the anode and, pre-eminently, in the bulk solution by homogeneous $^{\bullet}OH$ generated from Fenton's reaction (2). The value of pH 3.0 was chosen because it is optimal for this reaction, and it was not further regulated during the EF treatment. It is noteworthy that in these EC pre-treatments, the solutions were only mineralized by about 30 %, a value much smaller than that found operating at bench scale. For example, for AB14 solutions, Parsa et al. (2011) reported a 91 % dye and 87 % COD removal in the EC treatment with a bench-scale reactor, whereas lower abatement of 80 % dye and 64 % COD was obtained at pilot scale. The lower decay of organics concentration under our continuous-flow conditions can be ascribed to the smaller coagulation of the dye and its by-products as compared to the greater removal of these species by the larger amount of flocs originated at bench scale.

In EF, the amount of $^{\bullet}OH$ produced in the bulk from Fenton's reaction (2) depends on the Fe^{2+} concentration acting as the catalyst (Sirés and Brillas, 2021) and, for this reason, the content of this ion needs to be optimized. As can be seen in Fig. 6a, there is a gradual TOC decay with electrolysis time at all Fe^{2+} concentrations, using the conditioned EC-treated (i.e., 15 min) dye solution in 39.6 mM NaCl medium. The TOC decay was fast at the beginning of the EF treatments, but it was further inhibited due to the generation of more recalcitrant by-products. Moreover, the TOC abatement was slightly enhanced at higher Fe^{2+} content, and the best TOC removal in the sequential EC-EF process was of 68.2 % using 1.0 mM Fe^{2+} after 540 min of EF (see Table 2). Fig. 6b presents the increase of EC_{TOC} with electrolysis time for the above assays, which can be ascribed to the loss of organic load alongside the formation of more recalcitrant by-products like short-chain aliphatic carboxylic acids. Decreasing final EC_{TOC} values of 6.94, 5.24, 4.66 and 4.18 kWh (g TOC)$^{-1}$ were found at increasing Fe^{2+} concentrations of 0.10, 0.25, 0.50 and 1.0 mM (see Table 2). This tendency can be simply related to the progressive production of more $^{\bullet}OH$ from the acceleration of Fenton's reaction (2) due to the presence of more catalyst.

A similar behavior can be observed in Fig. 6c and d for the analogous

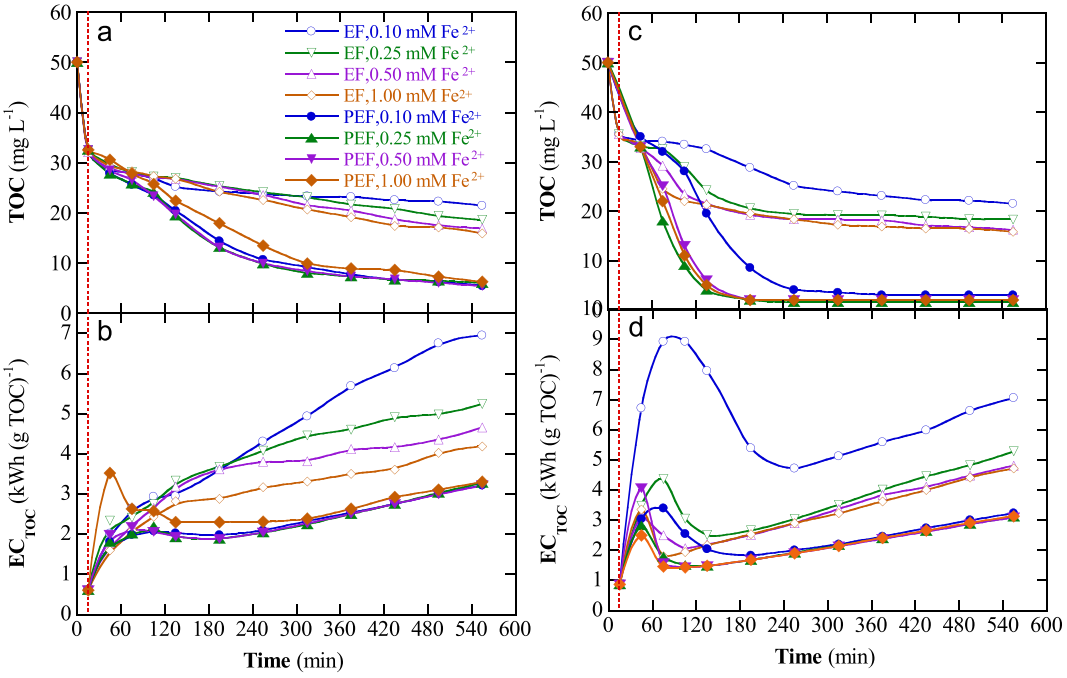

Fig. 6. Effect of Fe^{2+} concentration on (a,c) TOC removal and (b,d) energy consumption per gram of TOC over electrolysis time for the sequential EC-EF and EC-PEF treatments of solutions containing 50 mg L^{-1} TOC of AB14 dye in (a,b) 39.6 mM NaCl and (c,d) 20 mM Na_2SO_4 media. First, the solution at natural pH was treated by EC with the continuous-flow reactor of Fig. 1, with the 5A + 4C configuration at $I = 13.70$ A and liquid flow rate of 10 L h^{-1}, until steady conditions were reached after 15 min. The subsequent EF and PEF processes were applied in the recirculation plant of Fig. 2 for 540 min, employing 2.5 L of the EC-treated solution. EF and PEF conditions: solution conditioned at pH 3.0, addition of Fe^{2+} and application of a current density (j) of 50 mA cm^{-2}, at a liquid flow rate of 180 L h^{-1} and 35 °C. In PEF, a 125-W UVA lamp was placed inside the photoreactor for irradiation.

Table 2
Percentage of TOC removal and energy consumptions determined after: (i) The EC treatment of solutions containing 50 mg L^{-1} TOC of AB14 in 39.6 mM NaCl or 20 mM Na_2SO_4 at natural pH, with the 5A + 4C configuration at $I = 13.70$ A and liquid flow rate of 10 L h^{-1} for 15 min; and (ii) after 540 min of the sequential EC-EF or EC-PEF process with different Fe^{2+} concentrations at $j = 50$ mA cm^{-2}.

Medium	$[Fe^{2+}]$ (mM)	% TOC removal	EC_{TOC} (kWh (g TOC)$^{-1}$)	$EC_{TOC,total}$ [a] (kWh (g TOC)$^{-1}$)	EC_V (kWh m^{-3})	$EC_{V,total}$ [a] (kWh m^{-3})
EC process						
39.6 mM NaCl [b]	–	34.9	0.60	–	10.41	–
20 mM Na_2SO_4 [c]	–	28.9	0.86	–	12.47	–
Sequential EC-EF process						
39.6 mM NaCl [d]	0.10	57.3	6.94	–	79.57	–
	0.25	62.9	5.24	–	79.57	–
	0.50	66.3	4.66	–	79.57	–
	1.00	68.2	4.18	–	79.57	–
20 mM Na_2SO_4 [e]	0.10	57.0	7.04	–	86.27	–
	0.25	63.5	5.27	–	86.27	–
	0.50	67.6	4.80	–	86.27	–
	1.00	68.4	4.72	–	86.27	–
Sequential EC-PEF process						
39.6 mM NaCl [d]	0.10	89.2	3.22	13.26	79.57	469.67
	0.25	88.1	3.27	13.59	79.57	469.67
	0.50	89.4	3.21	13.23	79.57	469.67
	1.00	86.4	3.29	13.65	79.57	469.67
20 mM Na_2SO_4 [e]	0.10	93.1	3.23	12.47	86.27	476.27
	0.25	96.6	3.10	11.97	86.27	476.27
	0.50	96.7	3.08	11.92	86.27	476.27
	1.00	96.0	3.13	12.06	86.27	476.27

E_{cell}: [b] 7.6 V, [c] 9.1 V, [d] 19.2 V and [e] 20.5 V.
[a] Total energy consumption in PEF considering the electrical energy of the 125-W UVA lamp.

trials conducted with 20 mM Na_2SO_4. For the best trial, with 1.0 mM Fe^{2+}, 68.4 % of TOC was reduced in the sequential EC-EF treatment, quite similar to 68.2 % found in chloride medium. However, a slightly greater $EC_{TOC} = 4.716$ kWh (g TOC)$^{-1}$ was determined in sulfate medium (see Table 2). Note that maximum EC_{TOC} values were obtained at 60–90 min of the EF treatments (see Fig. 6d), attributed to the slow loss of TOC at the beginning of the processes that was further accelerated. Overall mineralization is very difficult in EF due to the degradation of the dye to final short-linear carboxylic acids, which form Fe(III)-carboxylate complexes that are very stable and persistent to the attack of oxidants (Thiam et al., 2014, 2018). Our results with the sequential EC-EF system are worse than those reported by Suhan et al. (2020) for hybrid EC-EF treatment of a Remazol Black B dye solution with Fe electrodes and Fe^{2+} and H_2O_2 addition, which yielded over 86 % of mineralization. Conversely, their EC process alone yielded a mineralization as low as 19.8 %, a value much smaller than that obtained with our system. This suggests that our EC configuration and the optimization steps implemented are better, leading to a superior EC system, whereas the H_2O_2 electrogeneration rate could be still improved to attain the mineralization values obtained by Suhan et al. (2020).

3.2.3. Sequential EC-PEF treatment of AB14 solutions

The EF treatment of the AB14 solutions showed that their TOC removal rate was determined by the concentration of the Fe^{2+} catalyst, which controls the rate of Fenton's reaction (2) for $^{\bullet}OH$ production. Based on that finding, the sequential EC-PEF processes was explored under the same conditions to assess the influence of the Fe^{2+} content under irradiation with a 125-W UVA lamp, and the results obtained are comparatively presented in Fig. 6. A faster TOC abatement can be seen in Fig. 6a and c in the PEF treatment as compared to EF trends, still observing a greater degradation at higher Fe^{2+} concentration. This behavior can be related to the acceleration of Fenton's reaction (2) thanks to the faster recycling of Fe^{2+}, leading to a quicker destruction of organics with a faster production of photoactive by-products that can be more rapidly photolyzed by UVA light, particularly the final Fe(III)-carboxylate complexes that are quickly photodecomposed. The best results were obtained with 0.50 mM Fe^{2+}, attaining a final TOC removal of 89.4 % and 96.7 % in chloride and sulfate matrices, respectively (see Table 2), whereas the final $EC_{TOC} = 3.21$ kWh (g TOC)$^{-1}$ obtained in chloride medium was higher than 3.08 kWh (g TOC)$^{-1}$ determined in sulfate solution (see Fig. 6b and d). Table 2 shows that the energy consumption was not significantly affected by the Fe^{2+} concentration. The superior mineralization in sulfate medium can be ascribed to the absence of refractory derivatives like chloro-organics, which are typically formed in chloride solutions from generated active chlorine and are known to be quite stable against Pt($^{\bullet}OH$), $^{\bullet}OH$ and UVA irradiation. These results agree with the excellent performance of the sequential EC-PEF process in batch mode reported by Thiam et al. (2014), reaching an almost overall mineralization of synthetic Tartrazine dye solutions. It should be noted that the final EC_{TOC} values found for both sequential treatments with PEF were much lower than the corresponding $EC_{TOC,total}$ ones determined when considering the nominal power of the UVA lamp (see Table 2). However, the calculated total energy consumption is just a first approach, since it actually depends on the lamp power and the energy loses. The use of free sunlight as an energy source can then be envisaged for the practical application of the sequential EC-PEF process.

4. Conclusions

It has been shown that the continuous-flow EC treatment with Fe electrodes is successful for color removal of AB14 diazo dye solutions, but it is insufficient for TOC destruction. The formation of flocs to coagulate organics depends on the experimental conditions. The best operation conditions were found with a 5A + 4C configuration, using aerated chloride medium within a pH interval from 4.0 to 10.0, $I = 13.70$ A and low liquid flow rate of 10 L h^{-1}. The process conditions for EC treatment in continuous mode, including the electrode configuration, were optimized. When the continuous-flow EC reactor was coupled to an EF recirculation system, at pH 3.0 and $j = 50$ mA cm^{-2}, near 68 % of TOC reduction was achieved regardless of the electrolyte composition. In contrast, about 90 % of TOC decay was attained in chloride medium, which was risen up to about 97 % in sulfate, when a sequential EC-PEF

treatment was studied. In both coupled treatments, the rise of added Fe^{2+} concentration at least up to 0.50 mM enhanced the TOC removal, whereas the superiority of PEF was due to the fast photolysis of final Fe(III)-carboxylate complexes formed upon irradiation with UVA light. The formation of recalcitrant chloroderivatives upon the attack of electrogenerated active chlorine limited the mineralization process in chloride solutions. In order to overcome the high energy consumption from UVA radiation in PEF, the use of natural sunlight is recommended in practice. Note that the results obtained in this work are limited to synthetic solutions only, and further studies are required to extend their validity to actual AB14 dye effluents.

CRediT authorship contribution statement

Ömür Gökkuş: Data curation, Investigation, Methodology, Validation, Writing – original draft. **Enric Brillas:** Formal analysis, Funding acquisition, Writing – original draft. **Ignasi Sirés:** Conceptualization, Funding acquisition, Project administration, Resources, Supervision, Writing – original draft, Writing – review & editing.

Declaration of competing interest

The authors declare that they have no known competing financial interests or personal relationships that could have appeared to influence the work reported in this paper.

Data availability

Data will be made available on request.

Acknowledgments

The authors gratefully acknowledge financial support from projects PID2019-109291RB-I00 and PID2022-140378OB-I00 (MCIN/AEI/10.13039/501100011033, Spain), as well as the contribution of Sergio Tena Sierra to the EC reactor design. Ö. G. would like to thank support from the International Post-Doctoral Research Fellowship Programme (Grant Number: 1059B191601343) funded by the Scientific and Technological Research Council of Türkiye (TUBITAK) 2219.

Appendix A. Supplementary data

Supplementary data to this article can be found online at https://doi.org/10.1016/j.scitotenv.2023.169143.

References

Akansha, J., Nidheesh, P., Gopinath, A., Anupama, K., Kumar, M.S., 2020. Treatment of dairy industry wastewater by combined aerated electrocoagulation and phytoremediation process. Chemosphere 253, 126652.

Akbal, F., Camcı, S., 2011. Copper, chromium and nickel removal from metal plating wastewater by electrocoagulation. Desalination 269, 214–222.

Badawi, A.K., Zaher, K., 2021. Hybrid treatment system for real textile wastewater remediation based on coagulation/flocculation, adsorption and filtration processes: performance and economic evaluation. J. Water Process Eng. 40, 101963.

Bassyouni, D.G., Hamad, H.A., El-Ashtoukhy, E.S.Z., Amin, N.K., El-Latif, M.M.A., 2017. Comparative performance of anodic oxidation and electrocoagulation as clean processes for electrocatalytic degradation of diazo dye Acid Brown 14 in aqueous medium. J. Hazard. Mater. 335, 178–187.

Benekos, A.K., Tziora, F.E., Tekerlekopoulou, A.G., Pavlou, S., Qun, Y., Katsaounis,. A, Vayenas, D.V., 2021. Nitrate removal from groundwater using a batch and continuous flow hybrid Fe-electrocoagulation and electrooxidation system. J. Environ. Manage., 297, 113387.

Bruguera-Casamada, C., Araujo, R.M., Brillas, E., Sirés, I., 2019. Advantages of electro-Fenton over electrocoagulation for disinfection of dairy wastewater. Chem. Eng. J. 376, 119975.

Chen, Z., Xia, P., Wang, D., Niu, X., Ao, L., He, Q., Wang, S., Ye, Z., Sirés, I., 2023. New insights into the mechanism of Fered-Fenton treatment of industrial wastewater with high chloride content: role of multiple reactive species. Sci. Total Environ. 882, 163596.

Cornejo, O., Murrieta, M.F., Castañeda, L.F., Nava, J.L., 2021. Electrochemical reactors equipped with BDD electrodes: geometrical aspects and applications in water treatment. Curr. Opinion Solid State Mater. Sci. 25, 100935.

Daniel, G., Zhang, Y., Lanzalaco, S., Brombin, F., Kosmala, T., Granozzi, G., Wang, A., Brillas, E., Sirés, I., Durante, C., 2020. Chitosan-derived nitrogen-doped carbon electrocatalyst for a sustainable upgrade of oxygen reduction to hydrogen peroxide in UV-assisted electro-Fenton wter treatment. ACS Sustain. Chem. Eng. 8, 14425–14440.

Dubrawski, K.L., van Genuchten, C.M., Delaire, C., Amrose, S.E., Gadgil, A.J., Mohseni, M., 2015. Production and transformation of mixed-valent nanoparticles generated by Fe(0) electrocoagulation. Environ. Sci. Technol. 49, 2171–2179.

Flores, N., Brillas, E., Centellas, F., Rodríguez, R.M., Cabot, P.L., Garrido, J.A., Sirés, I., 2018. Treatment of olive oil mill wastewater by single electrocoagulation with different electrodes and sequential electrocoagulation/electrochemical Fenton-based processes. J. Hazard. Mater. 347, 58–66.

Fu, X., Li, L., Yang, G., Xu, X., He, L., Zhao, Z., 2020. Removal of trace thallium from industrial wastewater by Fe^0-electrocoagulation. Water 12, 163.

Gholikandi, G.B., Kazemirad, K., 2018. Application of electrochemical-peroxidation process (ECP) for waste-activated sludge stabilization and system optimization using response surface methodology (RSM). Water Sci. Technol. 77, 1765–1776.

Gökkuş, Ö., Yıldız, Y.Ş., 2016. Application of electro-Fenton process for medical waste sterilization plant wastewater. Desal. Water Treat. 57 (56), 1–12.

Gökkuş, Ö., Yıldız, Y.Ş., Yavuz, B., 2012. Optimization of chemical coagulation of real textile wastewater using Taguchi experimental design method. Desalin. Water Treat. 49, 263–271.

Gurav, R., Bhatia, S.K., Choi, T.-R., Choi, Y.-K., Kim, H.J., Song, H.-S., Lee, S.M., Park, S. L., Lee, H.S., Koh, J., Jeon, J.-M., Yoon, J.-J., Yang, Y.-H., 2021. Application of macroalgal biomass derived biochar and bioelectrochemical system with Shewanella for the adsorptive removal and biodegradation of toxic azo dye. Chemosphere 264, 128539.

Hendaoui, K., Ayari, F., Rayana, I.B., Amar, R.B., Darragi, F., Trabelsi-Ayadi, M., 2018. Real indigo dyeing effluent decontamination using continuous electrocoagulation cell: study and optimization using response surface methodology. Process. Saf. Environ. Prot. 116, 578–589.

Heng, Z.W., Tan, Y.Y., Chong, W.C, Mahmoudi, E., Mohammad, A.W., Teoh, H.C, Sim. L. C., Koo, C.C., 2021.Preparation of a novel polysulfone membrane by incorporated with carbon dots grafted silica from rice husk for dye removal. J. Water Process Eng. 40, 101805.

İrdemez, Ş., Demircioğlu, N., Yildiz, Y.Ş., 2006. The effects of pH on phosphate removal from wastewater by electrocoagulation with iron plate electrodes. J. Hazard. Mater. 137, 1231–1235.

Jiang, W.-M., Chen, Y.-M., Chen, M.-C., Liu, X.-L., Liu, Y., Wang, T., Yang, J., 2019. Removal of emulsified oil from polymer-flooding sewage by an integrated apparatus including EC and separation process. Sep. Purif. Technol. 211, 259–268.

Keyikoglu, R., Can, O.T., Aygun,. A, Tek, A., 2019. Comparison of the effects of various supporting electrolytes on the treatment of a dye solution by electrocoagulation process. Colloid Interface Sci. Commun. 33, 100210.

Kobya, M., Gengec, E., Demirbas, E., 2016. Operating parameters and costs assessments of a real dyehouse wastewater effluent treated by a continuous electrocoagulation process. Chem. Eng, Process. Process Intens. 101, 87–100.

Kumar, A., Nidheesh, P.V., Suresh Kumar, M., 2018. Composite wastewater treatment by aerated electrocoagulation and modified peroxi-coagulation processes. Chemosphere 205, 587–593.

Louhichi, B., Gaied, F., Mansouri, K., Jeday .R., M, 2022. Treatment of textile industry effluents by electro-coagulation and electro-Fenton processes using solar energy: a comparative study. Chem. Eng. J. 427, 131735.

Maitlo, H.A., Kim, J.H., Kim, K.-H., Park, J.Y., Khan, A., 2019. Metal-air fuel cell electrocoagulation techniques for the treatment of arsenic in water. J. Clean. Prod. 207, 67–84.

Malakootian, M., Yousefi, N., Fatehizadeh, A., 2011. Survey efficiency of electrocoagulation on nitrate removal from aqueous solution. Int. J. Environ. Sci. Technol. 8, 107–114.

Mansor, E.S., Ali, H., Abdel-Karim, A., 2020. Efficient and reusable polyethylene oxide/polyaniline composite membrane for dye adsorption and filtration. Colloid Interface Sci. Commun. 39, 100314.

Mollah, M.Y.A., Pathak, S.R., Patil, P.K., Vayuvegula, M., Agrawal, T.S., Gomes, J.A.G., Kesmez, M., Cocke .L., D, 2004. Treatment of orange II azo-dye by electrocoagulation (EC) technique in a continuous flow cell using sacrificial iron electrodes. J. Hazard. Mater. 109, 165–171.

Moneer, A.A., El-Mallah, N.M., Ramadan, M.S.H., Shaker, A.M., 2021. Removal of acid green 20 and reactive yellow 17 dyes by aluminum electrocoagulation technique in a single and a binary dye system. Egyp. J. Aquat. Res. 47, 223–230.

Mousazadeh, M., Naghdali, Z., Al-Qodah, Z., Alizadeh, S.M., Karamati Niaragh, E., Malekmohammadi, S., Nidheesh, P.V., Roberts, E.P.L., Sillanpaa, M., Emamjomeh, M.M., 2021. A systematic diagnosis of state of the art in the use of electrocoagulation as a sustainable technology for pollutant treatment: an updated review. Sust. Energy Technol. Assess. 47, 101353.

Moussavi, G., Khosravi, R., Farzadkia, M., 2011a. Removal of petroleum hydrocarbons from contaminated groundwater using an electrocoagulation process: batch and continuous experiments. Desalination 278, 288–294.

Moussavi, G., Majidi, F., Farzadkia, M., 2011b. The influence of operational parameters on the elimination of cyanide from wastewater using the electrocoagulation process. Desalination 280, 127–133.

Mukhlish, M.B., Khan, M.R., Islam, M., Nazir, M., Snigdha, J., Akter, R., Ahmad, H., 2020. Decolorization of reactive dyes from aqueous solution using combined

coagulation-flocculation and photochemical oxidation (UV/H_2O_2). Sustain. Chem. Eng. 1, 51–61.
Nidheesh, P., Gökkuş, Ö., 2023. Aerated iron electrocoagulation process as an emerging treatment method for natural water and wastewater. Sep. Sci. Technol. 58, 2041-2063. Nidheesh, P.V..
Nidheesh, P.V., Scaria, J., Babu, D.S., Kumar, M.S., 2021. An overview on combined electrocoagulation-degradation processes for the effective treatment of water and wastewater. Chemosphere 263, 127907.
Othmani, A., Kesraoui, A., Seffen, M., 2017. The alternating and direct current effect on the elimination of cationic and anionic dye from aqueous solutions by electrocoagulation and coagulation flocculation. Euro-Medit. J. Environ. Integrat. 2, 6.
Parsa, J.B., Vahidian, H.R., Soleymani, A., Abbasi, M., 2011. Removal of Acid Brown 14 in aqueous media by electrocoagulation: optimization parameters and minimizing of energy consumption. Desalination 278, 295–302.
Pathak, A., Khandegar, V., Kumar, A., 2021. Removal of Acid Violet 17 by electrocoagulation using plain and extended surface electrodes. J. Hazard. Toxic Radioact. Waste 25, 06021002.
Rao, T., Ma, X., Yang, Q., Cheng, S., Ren, G., Wu, Z., Sirés, I., 2022. Upgrading the peroxi-coagulation treatment of complex water matrices using a magnetically assembled mZVI/DSA anode: insights into the importance of ClO radical. Chemosphere 303, 134948.
Ren, G., Lanzalaco, S., Zhou, M., Cabot, P.L., Brillas, E., Sirés, I., 2023. Replacing carbon cloth by nickel mesh as substrate for air-diffusion cathodes: H_2O_2 production and carbenicillin degradation by photoelectro-Fenton. Chem. Eng. J. 454, 140515.
Sakthisharmila, P., Palanisamy, P.N., Manikandan, P., 2018. Removal of benzidine based textile dye using different metal hydroxides generated in situ electrochemical treatment-a comparative study. J. Clean. Prod. 172, 2206–2215.
Shabestar, M.P., Moghaddam, M.R.A., Karamati-Niaragh, E., 2021. Evaluation of energy and electrode consumption of Acid Red 18 removal using electrocoagulation process through RSM: alternating and direct current. Environ. Sci. Pollut. Res. 28, 67214–67223.
Shokri, A., 2019. Application of electrocoagulation process for the removal of Acid Orange 5 in synthetic wastewater. Iran. J. Chem. Chem. Eng. 38, 113–119.
Simon, S., Suresh, B.K., Anantha-Singh, T., 2023. A sequential aerated electrocoagulation and peroxicoagulation process for the treatment of municipal stabilized landfill leachate by iron and graphite electrodes. Chemosphere 339, 139692.
Singh, S., Lo, S.-L., Srivastava, V.C., Qiao, Q., Sharma, P., 2021. Mineralization of perfluorooctanoic acid by combined aerated electrocoagulation and,odified peroxi-coagulation methods. J. Taiwan Inst. Chem. Eng. 118, 169–178.
Sirés, I., Brillas, E., 2021. Upgrading and expanding the electro-Fenton and related processes. Curr. Opin. Electrochem. 27, 100686.
Sonwani, R.K., Swain, G., Giri, B.S., Singh, R.S., Rai, B.N., 2020. Biodegradation of Congo red dye in a moving bed biofilm reactor: performance evaluation and kinetic modeling. Bioresour. Technol. 302, 122811.
Suhan, M.B.K., Shuchi, S.B., Anis, A., Haque, Z., Islam .S., M, 2020. Comparative degradation study of remazol black B dye using electro-coagulation and electro-Fenton process: kinetics and cost analysis. Environ. Nanotechnol. Monitor. Manage. 14, 100335.
Syam Babu, D., Nidheesh, P., Suresh Kumar, M., 2021. Arsenite removal from aqueous solution by aerated iron electrocoagulation process. Sep. Sci. Technol. 56, 184–193.
Thakur, L.S., Goyal, H., Mondal, P., 2019. Simultaneous removal of arsenic and fluoride from synthetic solution through continuous electrocoagulation: operating cost and sludge utilization. J. Environ. Chem. Eng. 7, 102829.
Thiam, A., Zhou, M., Brillas, E., Sirés, I., 2014. Two-step mineralization of Tartrazine solutions: study of parameters and by-products during the coupling of electrocoagulation with electrochemical advanced oxidation processes. Appl. Catal. Environ. 150-151, 116–125.
Thiam, A., Brillas, E., Centellas, F., Cabot, P.L., Sirés, I., 2015. Electrochemical reactivity of Ponceau 4R (food additive E124) in different electrolytes and batch cells. Electrochim. Acta 173, 523–533.
Thiam, A., Salazar, R., Brillas, E., Sirés, I., 2018. Electrochemical advanced oxidation of carbofuran in aqueous sulfate and/or chloride media using a flow cell with a RuO_2-based anode and an air-diffusion cathode at pre-pilot scale. Chem. Eng. J. 335, 133–144.
Tirado, L., Gökkuş, Ö., Brillas, E., Sirés, I., 2018. Treatment of cheese whey wastewater by combined electrochemical processes. J. Appl. Electrochem. 48, 1307–1319.
Titchou, F.E., Zazou, H., Afanga, H., El Gaayda, J., Akbour, R.A., Hamdanmi, M., Oturan, M.A., 2021. Electro-Fenton process for the removal of Direct Red 23 using BDD anode in chloride and sulfate media. J. Electroanal. Chem. 897, 115560.
Welcher, F.J., 1975. Standard methods of chemical analysis, 6th ed., vol. 2, part B. R.E. Krieger, publishing co, Huntington, New York, 1975.
Xiao, Z., Cui, T., Wang, Z., Dang, Y., Zheng, M., Lin, Y., Song, Z., Wang, Y., Liu, C., Xu, B., Ikhlaq, A., Kumirska, J., Siedlecka, E.M., Qi, F., 2022. Energy-efficient removal of carbamazepine in solution by electrocoagulation-electrofenton using a novel P-rGO cathode. J. Environ. Sci. 115, 88–102.
Yaseen, D.A., Scholz, M., 2019. Textile dye wastewater characteristics and constituents of synthetic effluents: a critical review. Int. J. Environ. Sci. Technol. 16, 1193–1226.
Ye, Z., Steter, J.R., Centellas, F., Cabot, P.L., Brillas, E., Sirés, I., 2019. Photoelectro-Fenton as post-treatment for electrocoagulated benzophenone-3-loaded synthetic and urban wastewater. J. Clean. Prod. 208, 1393–1402.
Yıldız, Y., Koparal, A.S., Keskinler, B., 2008. Effect of initial pH and supporting electrolyte on the treatment of water containing high concentration of humic substances by electrocoagulation. Chem. Eng. J. 138, 63–72.
Zampeta, C., Mastrantonaki, M., Katsaouni, N., Frontistis, Z., Koutsoukos, P.G., Vayenas, D.V., 2022. Treatment of printing ink wastewater using a continuous flow electrocoagulation reactor. J. Environ. Manage. 314, 115033.
Zodi, S., Merzouk, B., Potier, O., Lapicque, F., Leclerc, J.-P., 2013. Direct red 81 dye removal by a continuous flow electrocoagulation/flotation reactor. Sep. Purif. Technol. 108, 215–222.